Exploring the activity of a novel Au/TiC(001) model catalyst towards CO and CO_2 hydrogenation

Gian Giacomo Asara,[a,b] Josep M. Ricart,[a] Jose A. Rodriguez,[c] Francesc Illas[b]

[a] *Departament de Química Física i Inorgànica, Universitat Rovira i Virgili, C/ Marcel·lí Domingo s/n, 43007 Tarragona, Spain*

[b] *Departament de Química Física & IQTCUB, Universitat de Barcelona,*

C/ Martí i Franquès 1, 08028 Barcelona, Spain

[c] *Chemistry Department, Brookhaven National Laboratory Upton, NY 11973 (USA)*

Abstract

Small metallic nanoparticles supported on transition metal carbides exhibit an unexpected high activity towards a series of chemical reactions. In particular, the Au/TiC system has proven to be an excellent catalyst for SO_2 decomposition, thiophene hydrodesulfurization, O_2 and H_2 dissociation and the water gas shift reaction. Recent studies have shown that Au/TiC is a very good catalyst for the reverse water-gas shift ($CO_2 + H_2 \rightarrow CO + H_2O$) and CO_2 hydrogenation to methanol. The present work further expands the range of applicability of this novel type of systems by exploring the catalytic activity of Au/TiC towards the hydrogenation of CO or CO_2 with periodic density functional theory (DFT) calculations on model systems. Hydrogen dissociates easily on Au/TiC but direct hydrogenation of CO to methanol is hindered by very high activation barriers implying that, on this model catalyst, methanol production from CO_2 involves the hydrogenation of a HOCO-like intermediate. When dealing with mixtures of syngas ($CO/CO_2/H_2/H_2O$), CO could be transformed into CO_2 through the water gas shift reaction with subsequent hydrogenation of CO_2 to methanol.

Keywords: Syngas, methanol synthesis, CO, CO_2, Au/TiC, DFT

Introduction

The term "synthesis gas" (syngas) refers to the mixture of molecular hydrogen and carbon monoxide in various proportions. Syngas is obtained by steam reforming of coal and, hence, usually it also contains large amounts of carbon dioxide and small quantities of methane and water [1]. The massive use of syngas in industrial operations during the 20th century was triggered by the original work of Sabatier regarding the synthesis of methane from CO and molecular hydrogen [2]. This provides the basis for a subsequent valid alternative to petroleum derived fuels for the production of hydrocarbons especially through the Fischer-Tropsh process [3-5], discovered also nearly a century ago. The syngas is also the major feedstock for the synthesis of alcohols [6] and it is worth pointing out that methanol is one of the top ten industrial products. In both cases, Fischer-Tropsch and methanol synthesis, a suitable catalyst needs to be used. The Fischer-Tropsch synthesis is nowadays usually performed using modifications of the original Fe or Co based catalysts often supported on different types of oxides [7]. On the other hand, methanol synthesis is usually carried out with Cu/ZnO based catalysts at quite mild temperature and pressure conditions (220-300 °C and 50-100 bar) [6,8]. Additionally, direct hydrogenation of CO_2 is highly desirable to mitigate global warming caused by this greenhouse gas. Fortunately, recent advances seem to open promising perspectives [8].

In spite of these successful and widely used processes, the design of new active materials with improved performance for the conversion of syngas in valuables chemicals is still an active area of research, especially in view of the ever decreasing reserves of oil and the yet abundant coal deposits. It is important to point out that heterogeneous catalysts such as those used in the Fischer-Tropsch and methanol synthesis involve metallic particles of different size supported normally on oxides or sulfides and one may wonder whether a different chemistry would emerge by changing the support. Precisely, in the last decade a new family of catalysts has been proposed where the metal nanoparticles are supported on transition metal carbides (TMC) [9]. The idea to explore these systems comes from the combination of two apparently disconnected discoveries. On one hand the landmark paper of Levy and Boudard in the early 1970's [10] establishing the nowadays well-known noble metal-like behavior of early TMC, recovering many aspects of the surface reactivity of Pt, Ru or Rh, and, on the other hand the enormous interest in the catalytic properties of gold nanoparticles supported on oxides which, among other unexpected chemical properties [11,12], exhibit high activity for carbon monoxide oxidation at relatively low temperatures (200-350 K) [13-,22 the original discovered being due to the independent work of Haruta et al. [13] and Goodman et al. [21]. Clearly, merging the ideas behind the two discoveries by merging the two types of systems was quite a natural choice and a matter of time as discussed in a recent perspective article [9].The

first attempt to deposit Au nanoparticles on TMC surfaces involved the Au/TiC system. Initially, Roldan-Cuenya and coworkers investigated the interaction of Au nanoparticles with TiC films [23-25]. Later on, experiments for Au nanoparticles supported on TiC(001) single crystals carried out under well controlled ultra-high vacuum conditions complemented with theoretical calculations evidenced that the presence of the TiC support causes a strong modification of the electronic structure of the supported metal particles [26]. The TiC support strongly activates the deposited metal particle polarizing the electronic density above the nanoparticle thus facilitating the interaction with electron acceptor molecules. The larger effect corresponding to small nanoparticles involving one atomic layer only [27] and the effect of the TMC support also constitutes a non-trivial important issue [28]. The enhanced catalytic activity of admetals has been theoretically and experimentally confirmed on several systems. Thus, Au/TiC, and also Cu/TiC, have shown to be able to dissociate SO_2 [27,29] and to activate thiophene [30], which is subsequently decomposed in the presence of hydrogen. Au/TiC and Au/MoC constitute a new family of potential hydrodesulfuration catalyst [31]. Theoretical and experimental studies demonstrated that Au/TiC is able to dissociate molecular oxygen [32] and molecular hydrogen [33] with quite low energy barriers and, therefore, has significant catalytic activity. The dissociation of molecular oxygen is really surprising but not so useful because of the subsequent reaction of atomic oxygen with the underlying carbide leading to oxycarbide formation, especially at high temperatures [34,35] which ultimately degrades the system [36-39]. On the other hand, the facility of Au/TiC to dissociate molecular hydrogen strongly suggests that these systems could be excellent hydrogenation catalyst. Successive studies have addressed the different possible TMC-noble metal combinations which have been studied systematically [28,40,41].

To investigate the performance of Au/TiC, Cu/TiC and Ni/TiC as hydrogenation catalyst, experiments have been recently carried out on the possible conversion of CO_2 to methanol [42,43]. Experiments showed that, over these model catalysts, a mixture of CO, CH_4 and CH_3OH is produced. In all cases, CO is the major product, which is produced by the reverse water-gas shift (RWGS) reaction $CO_2 + H_2 \rightarrow CO + H_2O$. Nevertheless, a substantial amount of methanol is produced when using Au/TiC(001) and Cu/TiC(001), as shown in Figure 1, whereas methane is not detected. In the case of Ni/TiC(001), a mixture of CO, methanol, and methane is observed [44,45]. In line with previous work, the highest catalytic activity corresponds to small two-dimensional supported particles in close contact with the TiC(001) surface and periodic density functional theory based calculations points towards a HCOO carboxyl or carbon monoxide as the key intermediate [44,45]. Likewise, it is important to point out that the catalytic activity of the supported metals can be orders of magnitude higher than those of the extended Au(100), Cu(100), or Ni(100) surfaces.

Methanol synthesis over the industrial Cu/ZnO catalysts is known to proceed more efficiently on H_2/CO_2 than on H_2/CO mixtures [46] and there is evidence that the CO content in the syngas is converted to CO_2 through the water gas shift (WGS) reaction [6] although theoretical calculations show that direct CO hydrogenation takes place on Cu(111) [47]. Very recently, it has been shown that Au/TiC is a very good catalyst for the WGS reaction [48] but the possibility of direct hydrogenation of CO remains to be explored. Examining the experimental data in Figure 1, one can wonder if the methanol is produced by direct hydrogenation of a HOCO-like surface species or by hydrogenation of CO molecules formed during the RWGS. In the present work we first review the hydrogenation ability of Au/TiC and related systems and, second, present new results regarding precisely the direct hydrogenation of CO thus providing new insight into the fascinating chemistry of this new family of metal supported catalysts. Thus, the paper contains a summary of previous work which is needed to put the present results in the appropriate context and reports a series of new results regarding CO hydrogenation on TiC(001) and on TiC supported Au nanoparticles. To facilitate the discussion the two parts are clearly separated although general conclusions regarding all data reported are also given.

Brief review of H_2 dissociation and CO_2 hydrogenation on TiC(001) and Au/TiC(001)

In order to facilitate the discussion regarding hydrogenation of syngas on these novel model catalysts, it is convenient to briefly review previous work regarding two fundamental and related reactions. One concerns molecular hydrogen dissociation on TiC(001) and on Au/TiC(001) systems, a step providing a key reactant, and the other one involves the direct hydrogenation of CO_2 on these model catalysts.

Adsorption and dissociation of H_2 on TiC(001) and Au/TiC(001) systems

When studying syngas reactivity of the Au nanoparticle supported on TiC, a first necessary step concerns exploring the interaction of this model catalyst with atomic and molecular hydrogen. In fact it is well established that although H_2 dissociation does not spontaneously occur on extended perfect surfaces, it dissociates easily in presence of low coordinated gold atoms. This has been shown to be the case for extended systems as well as for isolated Au nanoparticles [49] and, later, for small Au nanoparticles supported on TiO_2 [50]. In a joint theoretical and experimental work, Florez *et al.* [33] reported a similar situation for H_2 interacting with Au/TiC; the effect of the size and shape of the supported metallic cluster on the hydrogen dissociation has been also studied in detail. These authors have shown that H_2 dissociates quite easily on the clean TiC(001) surface with an energy barrier of 0.52 eV only but have also found that small, flat, Au nanoparticles supported on TiC(001) can dissociate H_2 with even smaller barriers of 0.1 - 0.2 eV, depending on the particle

size [33]. Three different Au clusters supported on TiC(001) were considered, Au_4 and Au_9 both consisting of a single atomic layer on top of the TiC support and a larger Au_{13} cluster arranged in a 2-layers structure. The results obtained for H_2 dissociation demonstrated that the higher activity corresponds to the smaller Au_4 cluster, with a dramatic increase of the activation energy which passes from 0.08 eV for the smallest cluster to 0.2 eV on the Au_9 cluster reaching the value of ~1eV on the larger Au_{13} cluster. The atomic hydrogen produced spills over from the nanoparticle and diffuses on the carbide creating a reservoir of H atoms. Results identifying the highest activity for flat small nanoparticles can be rationalized in term of fraction of the noble metal in direct contact with the carbide support and in term of atomic coordination. For small flat nanoparticle the average coordination of the atoms decreases and, due to the interaction with the support, the polarization of the electronic density of the nanoparticle is stronger [26-28].

To further investigate the effect of the TMC support on the reactivity of Au nanoparticles, Florez et al. carried out a systematic theoretical study and compared adsorption and dissociation of H_2 on some Au_4/TMC systems (TMC = TiC, ZrC, VC, δ-MoC) [40]. The hydrogen molecule interacts rather strongly with the clean TiC(001) and ZrC(001) substrate, but quite weakly with VC(001) and δ-MoC(001). The first two carbides are the only ones supposed to be active catalysts for hydrogenation. In fact atomic hydrogen adsorption on surface carbon atoms of both VC and δ-MoC(001) causes an important distortion of the surface with a subsequent protrusion of the surface carbon out of the plane of the uppermost layer. The distortion resulting from the new C - H bond is predicted to destabilize the carbide. However on TiC, ZrC and δ-MoC clean (001) surfaces hydrogen dissociation seems to be possible because of its exothermicity (about -0.4 eV). The authors calculated a barrier of 0.80 eV for dissociation on ZrC (001), slightly larger than for TiC(001), a summary of results is reported in Table 1. To estimate the effect of the TMC support on the catalytic properties of Au nanoparticles, the Au_4 nanoparticle model already used in the study of Au/TiC [33] was chosen. The molecular hydrogen dissociation reaction on the Au_4 cluster deposited on all 4 TMC supports explored was found to be exothermic and the calculated activation barrier was always lower than 0.4 eV. The higher catalytic activity toward H_2 dissociation was seen for Au_4 cluster supported on ZrC(001) and TiC(001), the latter presenting a very low activation energy of ~0.1 eV.

Direct hydrogenation of CO_2 on TiC(001) and Au/TiC(001) systems

On the clean TiC(001) surface, CO_2 exhibits a moderate adsorption energy of -0.62 eV, forming a C-C bond and 2 O-Ti bonds with a concomitant activation of the molecule which passes from the linear geometry in the gas phase to a bent structure. On clean TiC(001), CO_2 direct hydrogenation was already studied by Viñes *et al*. as a fundamental elementary step of the water gas shift reaction [51]. However, in that case the reaction studied was in fact the dehydrogenation of HOCO although the microscopic reversibility of the process allows us to make use of those results to explore CO_2 reduction. On the clean TiC(001) surface, the co-adsorption of CO_2 and 2 hydrogen atoms is clearly exothermic with an adsorption energy larger than 1 eV. The calculated energy barrier to produce HOCO is of 0.8 eV which can be easily overcome at the experimental conditions. This elementary step is slightly endothermic with energy reaction of 0.3 eV. The HOCO adsorbed moiety has been recognized as a key intermediate of CO_2 hydrogenation because it can then evolve to methanol or to carbon monoxide after the cleavage of the HO-CO bond. CO formation implies to overcome a barrier of ~ 0.8 eV and it is exothermic by ~ 0.1 eV. Furthermore DFT calculations predict that the transition state for both first hydrogenation and CO formation after the cleavage of the HO-CO bond are well above the desorption limit. Therefore, CO_2 reduction will occur slowly confirming recent single crystal experiments [45], see also Figure 1. The situation changes after depositing Au on the TiC(001) surface at low coverage. Now CO_2 hydrogenation is boosted and both CO and methanol production become faster. Again, DFT calculations spread light and help understanding experimental data. In fact the information obtained studying the water gas shift reaction [48] can be used to analyze the experimental data that detected CO as the main product of CO_2 reduction (Figure 1). Using the smaller Au_4 cluster supported on TiC(001) we were able to study CO_2 adsorption and hydrogenation. The interaction with the Au supported nanocluster is somehow stronger than with the bare support and, consequently, CO_2 exhibits larger adsorption energy of about 0.7 eV. On the supported noble metal cluster the molecule is also significantly activated with a characteristic bent geometry and forming contemporarily one C - Au and one O – Au bonds with 2 different gold atoms.

On the supported Au_4 model cluster hydrogenation occurs with a very small activation barrier of 0.32 eV and the formation of HOCO is exothermic by 0.38 eV. A comparative energetic profile for CO_2 reduction on the Au_4/TiC(001) model system and on TiC(001) is shown in Figure 2 where reactants, transition state and products optimized structures for the HOCO formation are reported in Figure 3. Thus, the presence of the Au cluster causes a reduction of the activation barrier that passes from ~ 0.79 to ~ 0.32 eV producing a stable HOCO intermediate adsorbed on the supported Au_4 cluster. HOCO can be hydrogenated to form methanol or decompose into CO. On the Au_4/TiC(001) system the formation of CO involves the cleavage of one C-O bond of HOCO

and the production of Au-OH species. Indeed, those species are considered responsible for the considerable activity of small Au nanoparticles supported on oxides for the CO oxidation step of the water gas shift reaction [52]. The cleavage of one of the C-O bonds of HOCO to produce CO occurs overpassing an energy barrier of 0.94 eV. This activation energy is quite high but equilibrium is shifted to products by the fast production of HOCO. Furthermore CO interacts stronger with the carbide than with the gold cluster [63] and the molecules produced preferentially spill over the carbide instead of occupying of the Au active sites of the catalyst. These results predict that CO reduction to methanol will involve the production of CO_2 through the WGS reaction followed by the hydrogenation of HOCO. For comparison, a summary of the most important structural characteristic quantities for the reaction $CO_2 + H \rightarrow HOCO$ performed on the Au_4/TiC(001) model system are reported in Table 2.

Direct hydrogenation of CO on TiC(001) and Au/TiC(001) systems

This section describes new results regarding the direct hydrogenation of CO on these novel model catalysts. First, the different models used are described and computational details provided.

Material Models and Computational Details

The TiC(001) surface has been modeled by using slab model supercells of different sizes depending on the particular system used as discussed in previous works [26-33,36-45]; for additional details about the models we refer the reader to the recent perspective paper by Rodriguez and Illas [9]. To study the direct hydrogenation on CO on Au/TiC we used a $3(\sqrt{2} \times \sqrt{2})$ supercell with 4 layers, the two upper layers and the adsorbates were fully relaxed during the optimization whereas the bottom two ones frozen as in the bulk and using the optimized bulk parameter of 4.328 Å. In order to use realistic models, one needs to recall that STM experiments on Au/TiC reveal that at low Au coverage the majority of supported particles are small and almost flat [27,30]. Experiments also show that only small Au clusters with atoms in direct contact with the carbide substrate are catalytically active [27,30]. Accordingly, supported particles containing 4 and 6 atoms have been considered. The supercell of the model thus constructed contains 72 TiC units plus 4 or 6 Au atoms constituting the supported nanoparticle and CO and H_2 whenever needed (see Figure 4). The surface slab was separated by 10 Å vacuum from its images repeated along the z-axes avoiding self-interaction.

The theoretical results discussed in the present work were obtained by means of periodic density functional theory (DFT) based calculations using the VASP code [53,54]. The exchange and correlation contribution to the total DFT energy has been calculated using the PW91 form [55,56] of the generalized gradient approximation (GGA). Geometrical optimization of the adsorbate

structures has been performed using conjugate gradient or Newton-Raphson algorithms until forces on every relaxed atom were smaller than 0.02 eV/Å, where the energy threshold for convergence used was 10^{-6} eV. The valence electron density has been expanded using a plane wave basis set with an associated maximum kinetic energy of 415 eV. The effect of core electrons on the valence electron density has been taken into account through the projected augmented wave (PAW) method of Bloch [57] as in the implemented in VASP [58]. A 3×3×1 mesh of *k* points was generated using the Monkhorst-Pack algorithm [59] and subsequently used for numerical integration in the first Brillouin zone. For the purposes of the present work, this computational setup has proven to be sufficiently accurate [9,26-33,36-45].

Approximate transition state (TS) structures were initially guessed through the CI-NEB [60] method, refined using the Dimer method [61] and characterized by appropriate vibrational analysis. During the reaction the nature of the adsorbate interaction with the surface varies which also causes variations of the strength of the induced surface distortion [62]. For this reason it is crucial to include relaxation of the Au atoms during the TS search. Therefore, all energy differences have always been calculated between fully relaxed systems, this includes the two upper layers of the slab surface model, the supported Au_n (n=4,6) nanoparticles and the adsorbates. All adsorption energies reported are calculated as:

$$E_{ads} = E_{mol+surf} - E_{mol} - E_{surf}$$

where $E_{mol+surf}$ refers to the total energy of the relaxed surface and adsorbate: CO-TiC(001), CO-Au_n/TiC(001) (n=4,6) and 2H-CO-Au_n/TiC(001) (n=4,6); E_{mol} is the sum of the total energies of the gas phase molecules (CO and H_2), and E_{surf} is the total energy of the clean relaxed TiC(001) or the corresponding Au_n/TiC(001) (n=4,6) cell model. Within this formalism stable adsorption complexes result in negative adsorption energy values. The activation barrier and reaction energies of each elementary reaction step, E_{act} and E_{react}, have been calculated as usual from

$$E_{act} = E^{TS} - E^{IS}$$

$$E_{react} = E^{FS} - E^{IS}$$

here E^{TS} is the total energy of the transition state structure for an elementary reaction step that bring the system from an initial state whose total energy is E^{IS} to a final state with total energy E^{FS}.

Results and discussion

The high activity predicted for H_2 dissociation discussed in the preceding section and results obtained for CO_2 hydrogenation strongly suggest that the Au/TiC system would be a good catalyst for hydrogenation reaction involving syngas. To investigate this possibility, experiments and model

calculations explored the interaction of Au/TiC with CO_2/H_2 mixtures pointing out that small Au flat nanoparticles supported on TiC(001) are active catalysts for the RWGS and production of methanol. The Cu/TiC and Ni/TiC(001) model catalyst were also explored, Cu/TiC was shown to perform even better that Au/TiC whereas Ni/TiC demonstrated to be good for the production of methane [44,45]. Nevertheless, CO was produced always faster than methanol (Figure 1) supporting the idea that the reaction for methanol formation could occur after the RWGS on Au/TiC(001) [6]. In this case, CO_2 will be firstly transformed into CO and, in a subsequent step, the CO is hydrogenated in a sequential manner to produce methanol. In order to further investigate the plausibility of this mechanism we present a detailed study of the reduction of CO and CO_2 on TiC(001) and Au/TiC(001) which completes the picture drown by previous recent work [44,45].

As outlined above, low coordinated atoms of the Au nanoparticle are the active sites of the Au/TiC catalyst to dissociate H_2. The hydrogen atoms thus produced spill over the metal particle, populate the carbide support and, hence, are able to participate in hydrogenation reactions. On the other hand, there is evidence that CO adsorption is favored on smaller flat Au nanoparticles and that Au atoms in direct contact with the underline carbide provide the stronger interaction [63]. In each case, CO adopts on-top C-down geometry. However, one must point out that previous results regarding CO adsorption on Au/TiC(001) predicted stronger interaction with the surface carbons of the support respect to gold atoms [63]. Therefore, it is convenient to explore first the mechanism of CO hydrogenation on the clean TiC(001) surface. The experimental results in Figure 1 indicate that clean TiC(001) is able to catalyze the transformation of CO_2 into CO or methanol [45].

The interaction of CO with the TiC(001) surface involves directly the interaction with a C surface atom [62]. For a single CO molecules this results in an adsorption energy of -1.52 eV. Further dissociative adsorption of H_2 brings the system (containing one adsorbed CO and two adsorbed H atoms) 2.48 eV below the desorption level (Figure 5). Previous studies demonstrated that atomic hydrogen diffuses freely on the surface. However, CO diffusion from a C site to the closest Ti atom on TiC(001) is prevented by an energy barrier of 1.41 eV. The direct first hydrogenation of CO is often the rate limiting step in syngas reactivity on a variety of substrates with activation energy often higher than 1 eV due to the high stability of carbon monoxide. [64] On TiC(001) adding one H atom to CO leading to HCO is endothermic (+0.29 eV) and highly hindered by an activation energy of 1.92 eV. The reaction involves the coordination of the hydrogen with a Ti and a C atom of the surface as shown in Figure 6. No pathway was found for direct attachment of H to the oxygen atom of CO leading to a COH adsorbed species. The formation of a new O-H bond is possible only through HCO isomerization, but the process is endothermic by +0.85 eV and it is prevented by the extremely high energy barrier (2.91 eV). The addition of the second hydrogen

produces HCOH is endothermic by 0.79 eV and hampered by a very high energy barrier of 1.38 eV, similar to that calculated for the same reaction on other materials. In the transition state the H atom interacts simultaneously with the oxygen atom of HCO and surface C (Figure 7). No pathway was found for the addition of second hydrogen directly on the C atom. Clearly CO hydrogenation on the clean TiC(001) surface is unfavorable. Nevertheless, to complete the picture we have considered the possible isomerization of HCOH to formaldehyde (HCHO) by forming a second C-H bond. The process is predicted to be exothermic by -0.1 eV but the energy barrier calculated is again very high (1.84 eV) and the transition state structure, featuring a 3-membered-ring (Figure 8), is unstable respect to gas phase H_2 and CO by 0.44 eV. Thus, the overall route is hindered by high activation energy barriers. A summary of the reaction network studied on the clean TiC(001) surface is reported in Figure 9. In Figures 5 and 9, the large energy barrier for the first hydrogenation of CO is problematic since at an experimental level the barrier for the production of methanol from CO_2 hydrogenation on TiC(001) is in the order of 0.8-0.9 eV [45]. These results imply that the production of methanol via RWGS and then the subsequent hydrogenation of CO is not feasible. It is more likely a reaction pathway in which a HOCO intermediate, formed by hydrogenation of CO_2 [45], is somehow hydrogenated to yield methanol. Indeed, in Figure 1, the apparent activation energies for the formation of CO and methanol on TiC(001) are very similar (0.8-0.9 eV [45]) supporting the idea of a common key intermediate for the RWGS and methanol production. Selected geometrical parameters for the reaction on the clean support are reported in Table 3.

Let us now consider the direct hydrogenation of CO on the Au/TiC systems. Clearly, under a moderate CO partial pressure the TiC(001) surface will be covered with a certain amount of molecules and adsorption on Au nanoparticles will start to occur. From the preceding discussion it is clear that the contribution of the clean support to direct CO hydrogenation to methanol is negligible. Hence, in Figure 1, methanol has to be produced from CO hydrogenation on top of the supported Au nanoparticles or from direct hydrogenation of CO_2-like species. Since flat and small supported Au nanoparticles are more active than the three dimensional ones [9,43], the direct hydrogenation of CO on Au/TiC has been we modeled by considering two flat cluster models of 4 and 6 atoms supported on the TiC(001) slab model.

The supported Au_4 cluster has a square flat shape with gold atoms on top of surface carbon atoms as shown in Figure 2. The perpendicular Au-C distance for the optimized Au_4/TiC(001) model system is 2.128±0.005 Å where adjacent gold atoms remains 2.776 Å far apart. In our model study we focus on the attachment of the first hydrogen since this is likely to constitute the rate determining step of the overall hydrogenation process. On Au_4 CO adsorbs with moderate strength (-1.32 eV), C down, on top of a gold atom. Dissociative co-adsorption of H_2 brings the system -2.51

eV below the energy of the gas phase reactants (Figure 3). For convenience, in this structure one H atom is placed above the gold cluster where the second H atom remains far from the Au nanocluster on a surface carbon. HCO formation on top of the Au cluster is endothermic by 0.66 eV which shows that reduction will be disfavored but still possible. When the HCO species is adsorbed in its most favored geometry, C and O atoms interact with two first neighbor Au atoms. On the simple Au_4/TiC(001) model, the reaction proceeds with the attachment of the H atom to the carbon of CO and the subsequent approach of the oxygen to another gold atom. This mechanism requires the movement of the reactants over two nearly-perpendicular planes impeding the reaction. The corresponding transition state for this elementary step has been identified and characterized with just one imaginary frequency associated to the normal mode that brings the hydrogen atom from the gold atom to the carbon of CO that simultaneously tilts approaching the oxygen to the other gold atom. Structures of reactants, transition state and product are presented in Figure 8. The calculated energy barrier is 1.93 eV making this process hard to occur or almost impossible. However no other favorable mechanism has been identified for the reaction on top of the supported Au_4 cluster nor at the Au_4-TiC(001) interface.

The lack of activity of the Au_4 cluster is possibly due to the high distorted structure of a feasible transition state, imposed by approximate 4-fold symmetry of the supported cluster. To avoid this geometrical constrain a larger Au_6 cluster with the Au atoms adsorbed in two adjacent rows of surface carbons, has been constructed and optimized. The model now features two different kinds of Au atoms, those in the corner and those in the edge of the cluster. The average perpendicular distance between the Au atoms and the underlying C atoms of the surface is slightly smaller for corner Au (2.155 Å) than for those in the edge of the cluster (2.186), where the average distance separating the gold atoms is 2.773 ± 0.007 Å. Additional characteristic bond distances and angles of reactants, transition state and product structures optimized on the gold nanoparticle models are reported in Table 4 whereas activation and reaction energies for the first hydrogenation of CO and CO_2 on TiC(001) and on the 2 Au/TiC model systems used in this work are summarized in Table 5

Although the difference with the Au_4 model can seem subtle, adsorbate geometry and reaction mechanism can vary considerably. On Au_6/TiC(001) HCO resides on an edge atom of the supported cluster creating a new Au – C bond and with the oxygen pointing outside of the cluster Figure 9). This means that reduction of a CO molecule adsorbed on an edge atom can occur easily through attachment of atomic hydrogen adsorbed on the other row. In this case, hydrogen movement and CO tilting out of the cluster will occur on the same plane. Reactants, transition state and product identified for the reduction on the Au_6 gold cluster are sketched in Figure 9. However,

on this larger cluster the reaction is highly endothermic by 0.56 eV with high activation energy of 1.80 eV. This means that the Au_6 system is just slightly more active than the clean TiC (001) surface to reduce CO. The energy barrier decreases by 0.12 eV with respect to the clean TiC(001) surface and by 0.13 eV respect to Au_4 but they are still too large to provide the main route for syngas hydrogenation to methanol. In Figure 1, the apparent activation energy for the transformation of CO_2 into methanol is only 0.6 eV [45]. Several other reactive pathways have been considered (including reaction at the interface with diffusion of the hydrogen atom from and towards the surface of the support) but the reaction was found always highly unfavorable.

The present results together with experiments previously reported [44,45] indicate that HCO is unlikely to play a role on syngas hydrogenation. On the contrary, they highlight the important role played by the HOCO intermediate in CO_2 reduction to methanol. Therefore, one can conclude that CO hydrogenation on the clean TiC(001) surface and Au/TiC systems is highly disfavored by both thermodynamics and kinetics to the point that the reaction will not proceed. The formation and subsequent reduction of the carboxyl intermediate can be considered as the only process participating in methanol production from syngas mixtures ($CO/CO_2/H_2O/H_2$). Through the WGS, CO could be transformed into CO_2 and then hydrogenated to methanol.

Clearly, results presented in this section highlighted that hydrogenation reactions involving carbon monoxide are highly impeded on the clean TiC(001) support as well as on small supported Au nanoparticles. This leaves the hydrogenation of CO_2 – already present in synthesis gas feedstock or produced in water gas shift equilibrium conditions – as the most probable reactive pathway for methanol formation

General conclusions

Previous works presented compelling evidence that small gold nanoparticles supported on TiC provides an active catalyst for plenty of reactions like CO oxidation, O_2 dissociation, thiophene and SO_2 decomposition. This perspective paper reviews the catalytic properties of the Au/TiC system for hydrogenation reactions involving synthesis gas, a mixture of CO and hydrogen in various proportions with appreciable presence of CO_2 and water. In particular, we evaluated the performance of small Au clusters for hydrogen dissociation and hydrogenation of CO and CO_2 using periodic DFT calculations and suitable surface slab models.

The DFT results predict that H_2 dissociates easily on smaller supported Au cluster, highlighting the effect of the carbide support. In fact atoms in direct contact with the TiC(001) surface binds adsorbates stronger and in general dissociation occurs easier on smaller flat clusters. The atomic hydrogen spills over the carbide creating a reservoir that can in principle being used for

hydrogenation reaction. However, on Au_4/TiC(001), the CO direct hydrogenation is found to be highly hindered due to the high stability of the molecule and to the constrained geometry imposed by the gold cluster to the transition state leading to HCO formation. Unfortunately the situation does not change on the larger supported Au_6 cluster indicating that the hydrogenation reaction is unviable.

Despite of this lack of activity of Au/TiC towards CO hydrogenation, methanol can be produced if CO_2 is present in the syngas feedstock in agreement with recent experiments performed on model catalyst where CO was detected as primary product of CO_2 reduction together with an important production of methanol [45,46]. DFT results identified HOCO as a stable reaction intermediate on the Au/TiC catalyst and predict that CO reduction will occur with production of CO_2 through the reverse WGS reaction. CO_2 can then be hydrogenated easily and evolve to CO breaking one C-O bond or to methanol through subsequent hydrogenations.

Acknowledgments

G.-G. A thanks the Universitat Rovira i Virgili for supporting his predoctoral research. This work has been supported by the Spanish MINECO grants CTQ2012-30751 and CTQ2011-29054-CO2-01/BQU and, in part, by Generalitat de Catalunya grants 2014SGR97, 2014SGR199 and XRQTC. The work at BNL was financed by the US Department of Energy (DOE), Office of Basic Energy Science (DE-AC02-98CH10086). F.I. acknowledges additional support through the ICREA Academic award for excellence in research. Computational time at the MARENOSTRUM supercomputer has been generously provided by the Barcelona Supercomputer Centre through a grant from Red Española de Supercomputación.

Table 1 Molecular (E^{ads} (H_2)) and dissociative (E^{ads} (2H)) adsorption energy of H_2 on the Au_4 supported cluster and on the clean (001) surface of the transition metal carbide. Activation energy barrier (E^{act}) for the dissociation and energy variation (E^{react}) for the reaction: H_2(ads) → 2H(ads) are also reported. All values are in eV. Values are adapted from Ref. 33

TMC	E^{ads} (H_2) /eV	E^{ads}(2H) /eV	E^{act} /eV	E^{react}/eV
TiC(001)	-0.48	-0.91	0.52	-0.42
ZrC(001)	-0.66	-1.10	0.80	-0.44
VC(001)	0.04	0.28	-	0.24
δ-MoC(001)	0.04	-0.46	-	-0.42
Au_4/TMC				
TiC(001)	0.01	-1.10	0.08	-1.11
ZrC(001)	-0.24	-0.96	0.25	-0.72
VC(001)	0.01	-0.64	0.36	-0.65
δ-MoC(001)	-0.03	-0.54	0.34	-0.51

Table 2.- Characteristic structural quantities for reactants, transition state and product of the reaction: CO_2 + H → HOCO taking place on the Au_4/TiC model. Distances (*d*) are reported in Å. For a graphical explanation of the various quantities refer to Figure 11. The first of the two d(O-C) distances reported refers to the bond parallel to the surface.

	CO_2 + H	TS	HOCO
	2.131	2.269	2.259
d(O-C)	1.308; 1.217	1.388; 1.212	1.485; 1.202
d(Au-C)	2.138	2.100	2.069
d (Au-H)	1.613	1.802	-
d (H-O)	-	1.389	0.984

Table 3 Structural parameters of the optimized reactants, transition state and products for the direct hydrogenation of CO on the clean TiC(001) surface. Bond distances (*d*) are in Å and bond angles (α) in degrees. C_s refers to the surface C atom where each reactant is initially adsorbed (see Figure 4 for clarity).

	CO + H	TS	HCO
d(C-O)	1.195	1.232	1.294
d(C-C_s)	1.315	1.425	1.429
d(H-C_s)	1.125	1.605	-
d (H-Ti)	-	1.848	-
d (H-C)	-	1.443	1.112
α(HCO)	-	110.2	111.2

Table 4 Optimized bond distances and angles for reactants, transition state and product of the reaction: CO + H→HCO performed on the Au_4 and Au_6 nanoparticle models. Distances (*d*) are reported in Å and angles (α) in degrees.

Au_4/TiC(001)	CO + H	TS	HCO
d(C-O)	1.153	1.942	1.263
d(C-Au)	1.951	2.078	2.041
d(H-Au)	1.617	2.073	-
d(O-Au)	-	3.625	2.227
d(H-C)	-	1.295	1.112
α(HCO)	-	121.8	113.6
Au_6/TiC(001)			
d(C-O)	1.155	1.183	1.211
d(C-Au)	1.949	2.069	2.071
d(C-H)	-	1.361	1.118
d(H-Au)	1.611	1.864	-
α(HCO)	-	116.2	120.7

Table 5 Activation ($E_{ac}t$) and reaction (ΔE) energies for the first hydrogenation of CO and CO_2 calculated on the clean TiC(001) support and on the Au/TiC models used. Results for CO_2 have been adapted from [51] and [63]. All values reported are in eV.

Reaction	Substrate	ΔE	E_{act}
CO + H → HCO	TiC(001)	0.29	1.92
	Au_4/TiC(001)	0.66	1.93
	Au_6/TiC(001)	0.56	1.80
CO_2 + H → HOCO	TiC(001)	0.3	0.8
	Au_4/TiC(001)	-0.38	0.32

Figure 1: Arrhenius plots comparing the rates for the production of CO and methanol during the hydrogenation of CO_2 on clean TiC(001) and Au/TiC(001). CO was produced through the reverse water-gas shift reaction ($CO_2 + H_2 \rightarrow CO + H_2O$). The Au/TiC was prepared by depositing 0.1 ML of Au on the carbide substrate. In a batch micro-reactor, the catalysts were exposed to 0.049 MPa (0.5 atm) of CO_2 and 0.441 MPa (4.5 atm) of H_2. The reported values are for steady-state rates measured at temperatures of 600, 575, 550, 525 and 500 K.

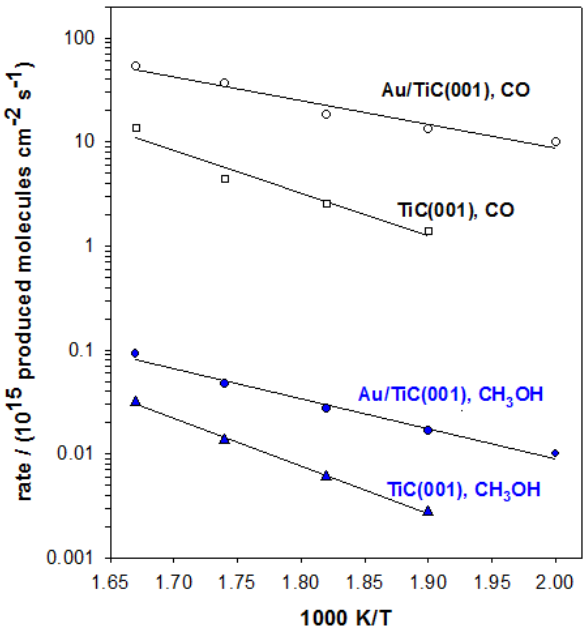

Figure 2: Comparative energetic profile for CO_2 hydrogenation on Au_4/TiC(001) (black line) and on the clean TiC(001) surface (red line, adapted from ref.[51**Error! Bookmark not defined.**]). Arrows represent the height of the activation barrier for the reaction on each substrate.

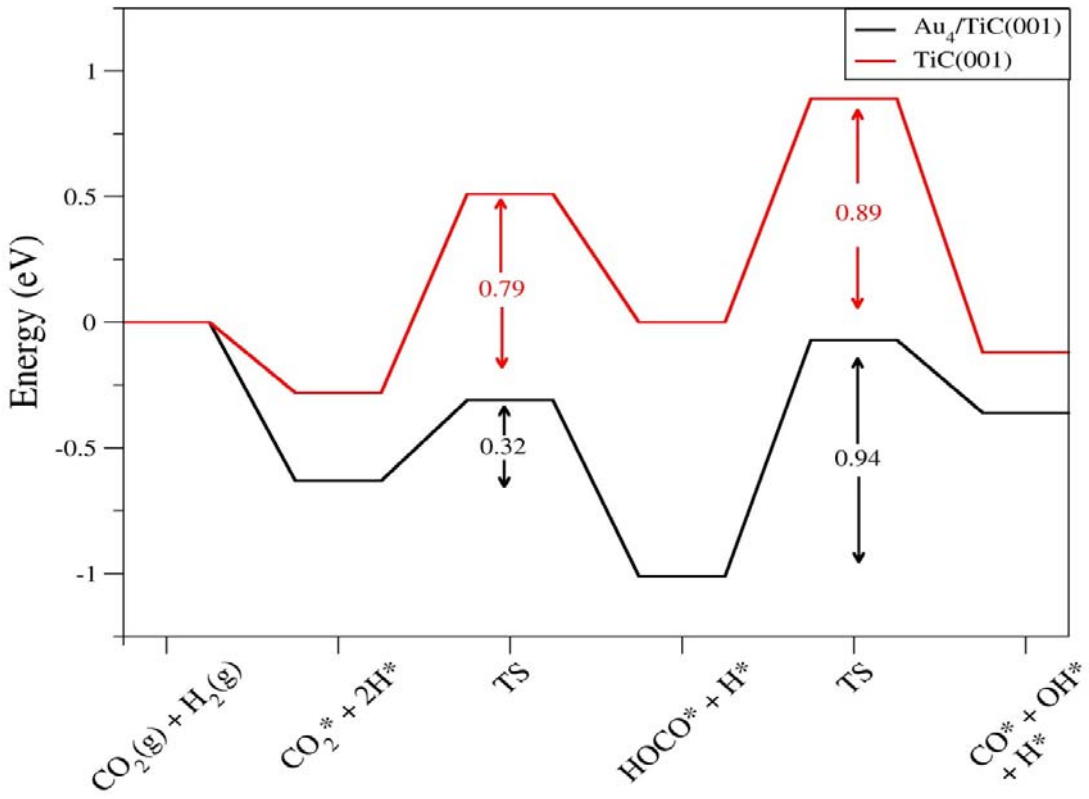

Figure 3: Side view (top figures) and top view (bottom figures) of the optimized structures of reactants, transition state and product for the first hydrogenation of CO_2 [$CO_2 + H \rightarrow HOCO$] on the Au_4/TiC(001) system as adapted from Ref. 48. On top of the gold cluster reduction CO_2 produces HOCO which is a stable intermediate. This can then evolve to methanol or to carbon monoxide. Color legend: Ti (grey), C (purple), O (red), H (white), Au **(**gold).

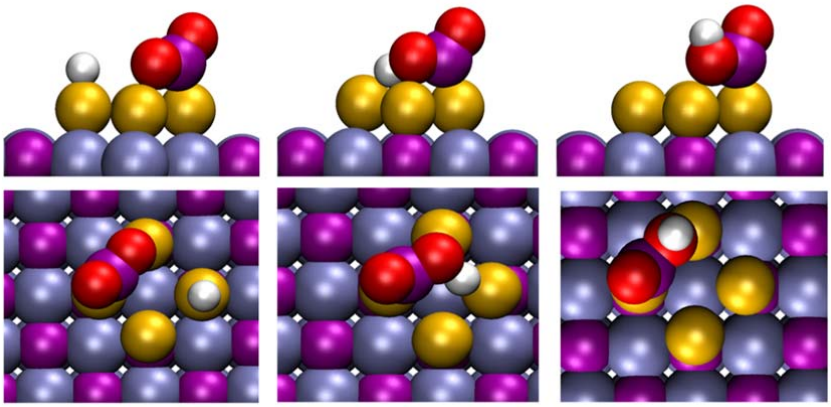

Figure 4: Top view (left) and side view (right) of the unit cell of the slab model used to reproduce the Au/TiC (001) model catalyst. In this case the Au_4 cluster model with one CO molecule and 2 H atoms (small white sphere, one on the Au cluster and one on the carbide) are represented. Gold atoms (yellow spheres) interact preferentially with surface carbons (cyan small spheres) and no one is in direct contact with surface Ti atoms (big grey spheres).

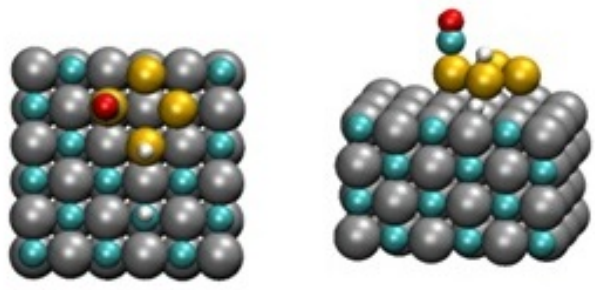

Figure 5: Comparative energy profile for CO and H_2 dissociative adsorption and of one hydrogen atom attachment to CO on the clean TiC (001) surface and on the two models of Au/TiC involving supported Au_4 and Au_6, respectively. Arrows represent the height of the activation energy barrier. All energies are in eV.

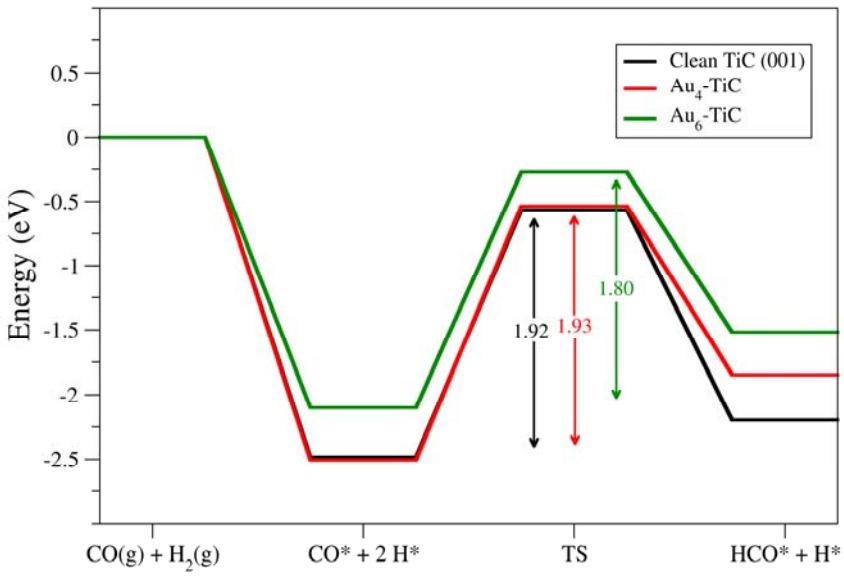

Figure 6: From left to right: reactants, transition state and product of the first hydrogenation of carbon monoxide [CO + H → HCO] on the clean (001) surface of TiC. Side and top view are sketched respectively in the upper and bottom part of the figure. Color legend: Ti (silver), C (cyan), O (red), H (white).

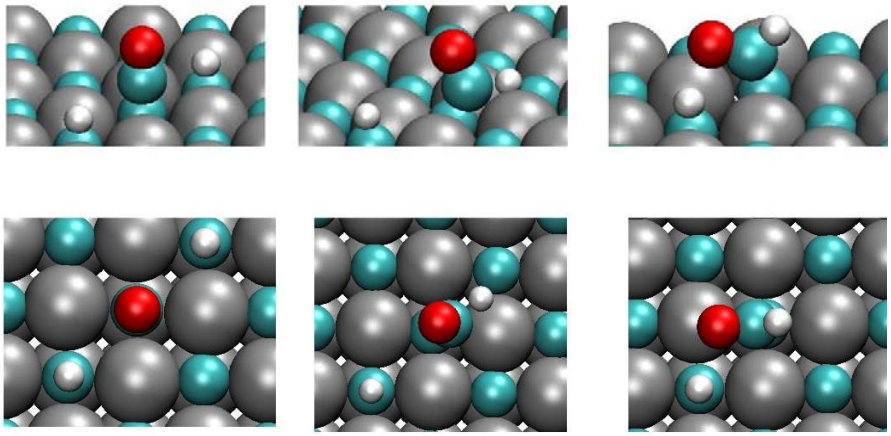

Figure 7: From left to right, reactants, transition state and product for the reaction: HCO + H → HCOH on the clean (001) surface of TiC. Side and top view are sketched respectively in the upper and bottom part of the figure. Colour legend: Ti(silver), C (cyan), O(red), H(white)

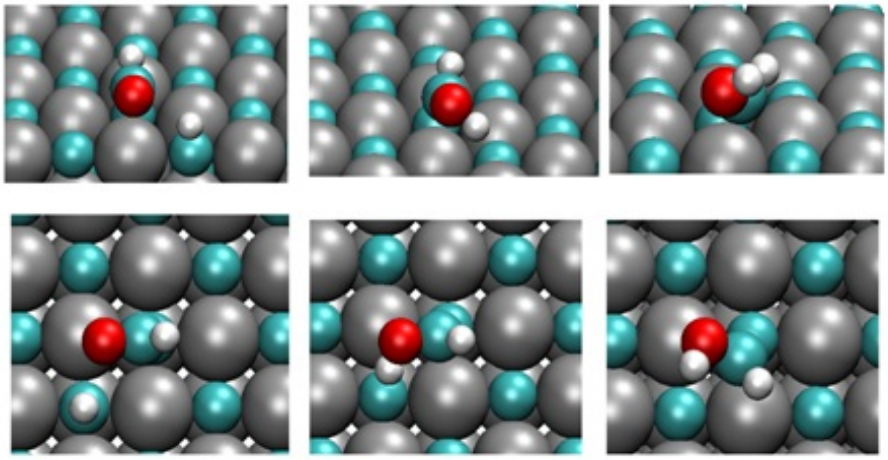

Figure 8: From left to right, reactants, transition state and product for the isomerization of HCOH to produce adsorbed formaldehyde (HCHO) on the clean (001) surface of TiC. Side and top view are sketched respectively in the upper and bottom part of the figure. Color legend: Ti (silver), C (cyan), O (red), H (white)

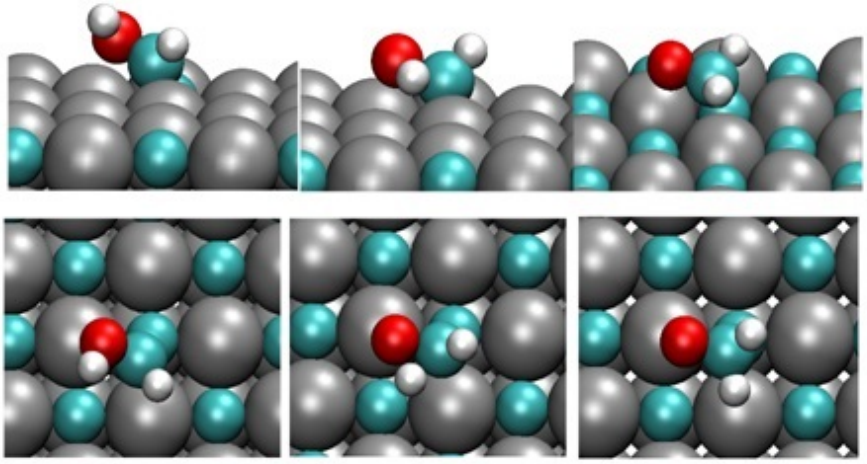

Figure 9: Calculated reactions network on the clean TiC (001) surface. In the model two adsorbed hydrogen atoms were explicitly included. Reaction energies (out of parenthesis) and activation barrier (in parenthesis) are reported in eV.

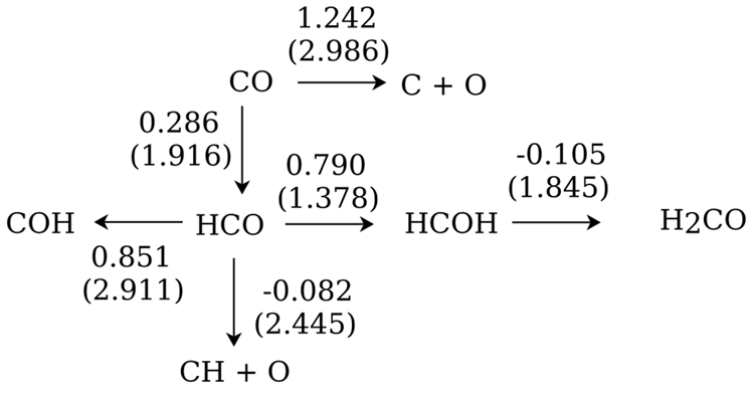

Figure 10: From left to right, reactants, transition state and product of the first hydrogenation of carbon monoxide [CO + H → HCO] on the smaller Au_4 nanoparticle model. Gold atoms are adsorbed on surface carbons in a 4-fold symmetry. Hydrogen diffuses from a neighboring gold atom, approaching the carbon monoxide. In the transition state H coordinates both gold atoms, CO tilts and oxygen goes closer to the gold atom that will coordinate HCO. Hydrogen transfer and CO tilting occur on nearly-perpendicular planes. Color legend: Ti (silver), C (cyan), O (red), H (white), Au (gold).

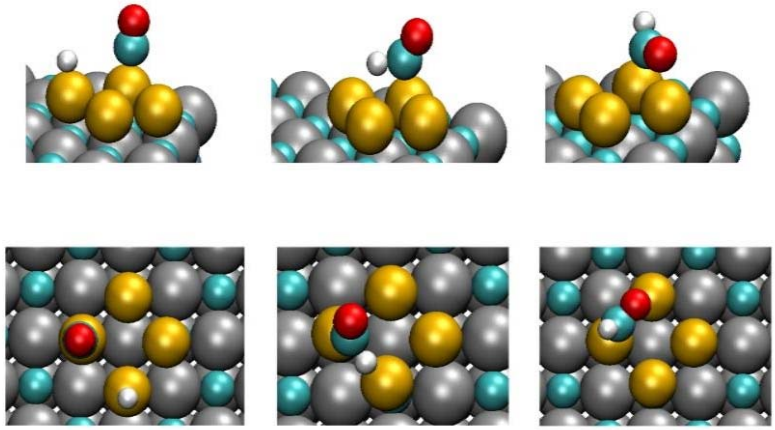

Figure 11: From left to right, reactants, transition state and product of the first hydrogenation of carbon monoxide [CO + H → HCO] on the bigger Au_6 nanoparticle model. Gold atoms are arranged in two rows, each atom directly interacting with a carbon of the surface. This geometry presents both edge and corner gold atoms, allowing a coplanar movement of reactants favoring the reaction. Color legend: Ti (silver), C (cyan), O (red), H (white), Au **(**gold).

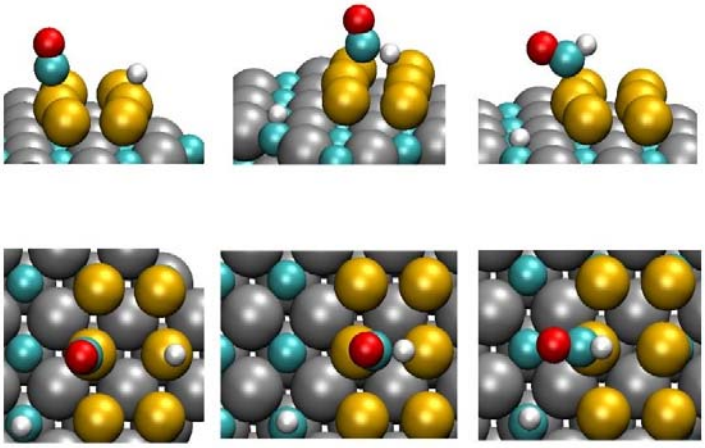

References

1. I. Wender, F. Proc. Tech., 48 (1996) 189.
2 P. Sabatier, J. B. Senderens, C. R. Hebd. Seances Acad. Sci., 134 (1902) 514.
3 F. Fischer, H. Tropsch, Brennstoff Chem., 4 (1923) 276.
4. F. Fischer, H. Tropsch, Brennstoff Chem., 7 (1926) 79.
5. F. Fischer, H. Tropsch, Chem. Ber., 59 (1926) 830.
6. G. W. Huber, S. Iborra, A. Corma, Chem. Rev., 106 (2006) 4044.
7. A. Y. Khodakov, W. Chu, P. Fongarland, Chem. Rev., 107 (2007) 1692.
8. W. Wang, S. Wang, X. Ma, J. Gong, Chem. Soc. Rev., 40 (2011) 3703.
9. J. A. Rodriguez, F. Illas, Phys. Chem. Chem. Phys., 14 (2012) 427.
10. R. B. Levy, M. Boudart, Science ,181 (1973) 547.
11. M. Haruta, N. Yamada, T. Kobayashi, S. Iijima, J. Catal., 115 (1989) 301.
12. M. S. Chen, D. W. Goodman, Science, 306 (2004) 252.
13. M. Haruta, Catal. Today, 36 (1997) 153.
14. M. S. Chen, D.W. Goodman, Science, 306 (2004) 252.
15. C. T. Campbell, S. C. Parker, D. E. Starr, Science, 298 (2002) 811.
16. L. M. Molina, B. Hammer, Appl. Catal. A: General, 291 (2005) 21.
17. A. Vijay, G. Mills, H. Metiu, J. Chem. Phys., 118 (2003) 6536.
18. I. N. Remediakis, N. Lopez, J. K. Nørskov, Angew. Chem. Int. Ed., 117 (2005) 1858.
19. J. Guzman, S. Carrettin, J. C. Fierro-Gonzalez, Y. Hao, B. C. Gates, A. Corma, Angew, Chem. Int. Ed., 117 (2005) 4856.
20. N. Cruz Hernández, J. F. Sanz, J. A. Rodriguez, J. Am. Chem. Soc., 128 (2006) 15600.
21. M. Walden, X. Lai, D. W. Goodman, Science, 281 (1998) 1647.
22. O. Meerson, G. Sitja, C. R. Henry, Eur. Phys. J. D., 34 (2005) 119.
23. L.K. Ono, D. Sudfeld, B. Roldan Cuenya, Surf. Sci., 600 (2006) 5041.
24 A. Naitabdi, L. K. Ono, B. Roldan-Cuenya, Applied Phys. Lett., 89 (2006) 043101.
25. L.K. Ono, B. Roldan-Cuenya, Catal. Letters, 113 (2007) 86.
26. J. A. Rodriguez, P. Liu, F. Vines, F. Illas, Y. Takahashi, K. Nakamura, J. Chem. Phys. 127 (2007) 211102.
27. J. A. Rodriguez, P. Liu, F. Viñes, F. Illas, Y. Takahashi, K. Nakamura, Angew. Chem. Int. Ed., 47 (2008) 6685.
28 E. Florez, L. Feria, F. Vines, J. A. Rodriguez, F. Illas, J. Phys. Chem. C, 113 (2009) 19994.
29. L. Feria, J. A. Rodriguez, T. Jirsak, F. Illas, J. Catal., 279 (2011) 352.

30. J. A. Rodriguez, P. Liu, Y. Takahashi, K. Nakamura, F. Viñes and F. Illas, J. Am. Chem. Soc., 131 (2009) 8595.
31. J. A. Rodriguez, P. Liu, Y. Takahashi, F. Viñes, L. Feria, E. Florez, K. Nakamura, F. Illas, Catal. Today, 166 (2011) 2.
32. J. A. Rodriguez, L. Feria, T. Jirsak, Y. Takahashi, K. Nakamura, F. Illas, J. Am. Chem. Soc., 132 (2010) 3177.
33. E. Florez , T. Gomez, P. Liu, J. A. Rodriguez, F. Illas, ChemCatChem, 2 (2010) 1219.
34. H. Kitaoka, K. Ozawa, K. Edamoto, S. Otani, Surf. Sci., 511 (2002) 359.
35. Y. Shirotori, K. Sadawa, K. Ozawa, K. Edamoto, S. Otani, Surf. Sci. 584 (2005) 237.
36. J. A. Rodriguez, P. Liu, J. Gomes, K. Nakamura, F. Viñes, C. Sousa, F. Illas, Phys. Rev. B, 72 (2005) 075427.
37. Y. F. Zhang, F. Viñes, Y. J. Xu, Y. Li, J. Q. Li, F. Illas, J. Phys. Chem. B, 110 (2006) 15454.
38. F. Viñes, C. Sousa, F. Illas, P. Liu, J. A. Rodriguez, J. Phys. Chem. C, 111 (2007) 1307.
39 F. Viñes, C. Sousa, F. Illas, P. Liu, J. A. Rodriguez, J. Phys. Chem. C, 111 (2007) 16982.
40. E. Florez, T. Gomez, J. A. Rodriguez, F. Illas, Phys. Chem. Chem. Phys., 13 (2011) 6865.
41. T. Gomez, E. Florez, J. A. Rodriguez, F. Illas, J. Phys. Chem. C, 115 (2011) 11666.
42. A. B. Vidal, L. Feria, J. Evans, Y. Takahashi, P. Liu, K. Nakamura, F. Illas, J. A. Rodriguez, J. Phys. Chem. Lett., 3 (2012) 2275.
43. J. A. Rodriguez, J. Evans, L. Feria, A. B. Vidal, P. Liu, K. Nakamura, F. Illas, J. Catal. 307 (2013) 162. Note that the reaction energy and activation barrier reported in this reference for CO2 + H → HOCO actually refer to the inverse process: HOCO → CO2 + H.
44. A. B. Vidal, L. Feria, J. Evans, Y. Takahashi, P. Liu, K. Nakamura, F. Illas, J. A. Rodriguez, J. Phys. Chem. Lett., 3 (2012) 2275.
45. J. A. Rodriguez, J. Evans, L. Feria, A. B. Vidal, P. Liu, K. Nakamura, F. Illas, J. Catal. 307 (2013) 162. Note that the reaction energy and activation barrier reported in this reference for CO2 + H → HOCO actually refer to the inverse process: HOCO → CO2 + H.
46. K. Klier, V. Chatikavanij, R. G. Herman, G. W. Simmons, J. Catal., 74 (1982) 343.
47 L. C. Grabow, M. Mavrikakis, ACS Catalysis 1 (2011) 365
48. J. A. Rodriguez, P. J. Ramírez, G. G. Asara, F. Viñes, J. Evans, P. Liu, J. M. Ricart, F. Illas, Angew. Chem. Int. Ed., 126 (2014) 11452.
49 A. Corma, M. Boronat, S. González, F. Illas, Chem. Commun., (2007) 3371.
50 M. Boronat, F. Illas, A. Corma, J. Phys. Chem. A, 113 (2009) 3750.
51 F. Viñes, J. A. Rodriguez, P. Liu, F. Illas, J. Catal., 260 (2008) 103.
52 M. Flytzani-Stephanopoulos, Acc. Chem. Res., 47 (2014) 783.

53. G. Kresse, J. Hafner, Phys. Rev. B, 47 (1993) 558.
54. G. Kresse, J. Furthmuller, Phys. Rev. B, 54 (1996) 11169.
55. J. P.Perdew, K. A. Jackson, M. R Pederson, D. J Singh, C. Fiolhais, Phys. Rev. B, 46 (1992) 6671.
56. J. P. Perdew, Y. Wang, Phys.Rev. B, 45 (1992) 244.
57. P. E. Blöchl, Phys. Rev. B, 50 (1994) 17953.
58. G. Kresse , D. Joubert, Phys. Rev. B, 59 (1999) 1758.
59. H. J. Monkhorst, J. D. Pack, Phys. Rev. B, 13 (1976) 5188.
60 G. Henkelman, B. P. Uberuaga, H. Jónsson, J. Chem. Phys., 113 (2000) 9902.
61 G. Henkelman, H. Jónsson, J. Chem. Phys., 111 (1999) 15.
62. B. Mant, G. G. Asara, J. A. Anderson, N. Homs, P. Ramirez de la Piscina, S. Rodriguez, J. M. Ricart, F. Illas, Surf. Sci., 613 (2013) 63.
63 G. G. Asara, L. Feria, E. Florez, J. M. Ricart, P. Liu, J. A. Rodriguez, F. Illas, J. Phys. Chem. C, 115 (2011) 22495.
64 P. Liu, Y. Choi, Y. X. Yang, M. G. White, J. Phys. Chem. A, 114 (2010) 3888.